Electronic Supplementary Material (ESI) for Physical Chemistry Chemical Physics.

Supporting Information

Title: Hygroscopic behavior and chemical reactivity of aerosols generated from mixture solutions of low molecular weight dicarboxylic acids and NaCl

Authors: Xue Li[+], Li Wu[+], Ji-Soo Lee, and Chul-Un Ro[*]

Department of Chemistry, Inha University, Incheon 22212, Korea

[+] Authors with equal contributions

[*] ***Correspondence to*** Chul-Un Ro (curo@inha.ac.kr)

A. Summary of hygroscopic behavior and chemical evolution of NaCl-MA mixture aerosols

Hygroscopic behavior and Raman spectra of malonic acid (MA), monosodium malonate (MSM), and disodium malonate (DSM) aerosols can be found in Li et al[1]. Fig. S1(A)-(C) plot the hygroscopic curves of particles with mixing ratios of NaCl:MA = 2:1, 1:1, and 1:2 as a function of the relative humidity (RH) along with chemical compositions and optical images. The hygroscopic behavior of droplets generated from the solutions of NaCl:MA = 2:1, 1:1, and 1:2 was as follows: (i) single-stage efflorescence and deliquescence; (ii) single-stage efflorescence and continuous growth; and (iii) continuous shrinkage and growth during the dehydration and humidification processes, respectively. During the dehydration process, as shown in Fig. S1(A), a droplet generated from an aqueous solution of NaCl:MA = 2:1 shrank continuously with decreasing RH and effloresced at RH = 44.8%. During the humidification process, the aerosol began to dissolve at RH = ~65% and deliquesced at RH = 73.2%. For all aerosols on an optical image field, their efflorescence RHs (ERHs) and deliquescence RHs (DRHs) were 39.4-44.8% and 73.2(±0.3)%, respectively. As shown in Fig. S1(B), the droplet generated from the NaCl:MA = 1:1 solution showed an ERH = 32.5% during the dehydration process, and all the aerosols on an optical image field showed their ERHs = 28.3-33.5%.

As shown in Fig. S1(D)-(F), the top Raman spectra of the droplets acquired at RH = 87.0%, 89.2%, and 84.5% immediately after generation from solutions of NaCl:MA = 2:1, 1:1, and 1:2, respectively, showed peaks at 1730 cm^{-1} (C=O vibration of -COOH group), 1406 cm^{-1} (CH_2 bending), and 1375 cm^{-1} (C=O vibration of $-COO^-$ group), indicating the presence of aqueous MA and hydrogen malonate (HMa^-) species formed from the reaction between MA and Cl^-. The second and third spectra in Fig. S1(D)-(F), appear similar to the top spectra, except for the increase in the peak intensities at 1375 and 1406 cm^{-1} relative to that at 1730 cm^{-1} and the decrease in the free water peak at 3430 cm^{-1}, indicating the further formation of HMa^- species.

The rest Raman spectra in Fig. S1(D)-(F) for aerosols from solutions of NaCl:MA = 2:1, 1:1, and 1:2, obtained at RH = 41.7-9.1%, 31.9-8.5%, and 19.7-6.1%, respectively, during the dehydration process, and at RH = 9.1-84.4%, 8.5-85.5%, and 6.1-88.4%, respectively, during the humidification process, show that with the further formation of the HMa^- the free water peaks at 1640 and 3430 cm^{-1} gradually decreased and increased during the dehydration and humidification process, respectively, indicating that the organic moieties are in the amorphous solid phase after

efflorescence.[2] The MA and MSM species desorb and absorb free water continuously during the dehydration and humidification processes, respectively, whereas the efflorescence and deliquescence events can be captured based on the size change when the NaCl content is considerable. As NaCl is very hygroscopic,[1] the 2-D area ratios of the droplets for the aerosols from the NaCl:MA solutions at the start of the dehydration process are larger than those at the end of the humidification process due to the consumption of NaCl (Fig. S1(A)-(C)). The comparison of hygroscopicity of NaCl-MA particles in the present and previous studies can be found in Li et al.[1]

B. Literature summary, including the present study, of the hygroscopic behavior of oxalic acid (OA) aerosols

For OA particles, the reported thermodynamic models and bulk solution measurements showed DRH > 97%.[3-6] Many studies also reported that the deliquescence of OA particles could not be experimentally observed at RH < 95%, as shown in Table S2,[4, 7-9] which is consistent with the present study. On the other hand, several HTDMA studies reported continuous hygroscopic growth of OA particles without clear deliquescence at RH > 10%.[2, 10, 11] The different observations might be because submicron (100 nm) aerosols investigated in the HTDMA works would exhibit different hygroscopic behavior to supermicron ones.[12] However, another HTDMA work showed no water uptake of OA particles at RH < 90%,[7] suggesting that the initial phase of dried OA particles passing through a diffusion dryer, either crystal or amorphous phase, is another factor leading to no deliquescence or continuous growth, respectively, except for size of the particles.[2, 10] Only a few studies have examined the hygroscopic behavior during the dehydration process of OA particles, as summarized in Table S2. One study reported the continuous shrinkage of OA aerosols at RH = 95-40% using HTDMA because gel-like structure was observed.[2] Additionally, studies of levitated OA droplets using the EDB (electro-dynamic balance) technique and OA droplets deposited on a polytetrafluoroethylene (PTFE) substrate using RMS reported different ERHs of 51.8 - 56.7% and 71%, respectively.[9, 13] The levitated OA droplets crystallized into anhydrous OA solids by considering the mass difference before and after efflorescence and it was proposed that the supersaturated droplets at low RHs do not have sufficient water to form OA dihydrate.[13] On the other hand, OA droplets deposited on PTFE substrates effloresced into OA

dihydrate,[9] which is the same as the present observation. The different ERHs between levitated and deposited OA droplets might be because of the use of the collecting substrates, which could facilitate the efflorescence.[9, 14, 15]

In this study, solid phase transitions between anhydrous OA and OA dihydrate were observed at RH = 20-40% and RH < 5% during the humidification and dehydration processes, respectively. Previous studies reported that anhydrous OA changed to OA dihydrate during the humidification process at RH = ~20%,[8] RH = 10-30%,[3] and RH = 17.9-19.6%,[9] which are comparable to the present observations. During the dehydration process, a transition from OA dihydrate to anhydrous OA at RH = ~5% was also reported with negligible change in size of the particle.[8, 9] Nevertheless, in this study, the anhydrous OA particles sublimed during the solid phase transition.

C. Hygroscopic behavior and Raman spectra of succinic acid (SA), monosodium succinate (MSS), and disodium succinate (DSS) aerosols

SA droplets effloresced into SA crystals at ERH = 84.4-90.1% as shown in Fig. S2(A) and (D), which is higher than ERH = 55-59% observed by an EDB study,[13] probably due to the substrate effects. The top Raman spectrum in Fig. S2(D) corresponds to the aqueous SA droplet at RH = 90% with characteristic peaks at 1404, 1708, and 2932 cm^{-1} for aqueous SA and 3450 cm^{-1} for free water, where the peaks at 1404 cm^{-1} and 2932 cm^{-1} were assigned to CH_2 bending and stretching vibrations, respectively, and the peak at 1708 cm^{-1} was for a C=O stretching of the -COOH group.[16] The bottom Raman spectrum in Fig. S2(D) is for the effloresced particle at RH = 5% and also for the standard SA powders, where the peaks at 1407, 1642, and 2920 and 2960 cm^{-1} are for the CH_2 bending vibration, C=O stretching vibration of -COOH group, and CH_2 stretching vibration, respectively.[17] During the humidification process, the morphology and Raman spectra of the particle did not change until RH = 95%. The DRH for bulk SA was reported to be 98.8%, and as summarized in Table S3, all of the previous studies reported DRH > 90%.[7, 11, 13, 18, 19]

As shown in Fig. S2(B), during the dehydration and humidification processes, a MSS droplet shrank and grew continuously as the RH was decreased from 95% to 5% and increased from 5% to 92%, respectively. The top and middle Raman spectra in Fig. S2(E) correspond to the aqueous and amorphous MSS aerosols at RH = 90% and 5%, respectively, which are the same as

each other except for the free water peak at 3450 cm^{-1}. The characteristic peaks of the aqueous and amorphous MSS particles were observed at 1404 cm^{-1} both for the CH_2 bending and C=O stretching of $-COO^-$ group, at 1706 cm^{-1} for the C=O stretching vibration of the -COOH group, and at 2932 cm^{-1} for the CH_2 stretching vibration.[16] As aqueous SA has two -COOH and aqueous MSS has one -COOH and one $-COO^-$, the peak intensity ratios at 1404 and 1706 cm^{-1} are different between the aqueous SA and MSS, which is useful for distinguishing them. The bottom Raman spectrum in Fig. S2(E) corresponds to crystalline MSS powders prepared by the evaporation of a MSS solution in a desiccator for several days, where the peaks at 1260, 1407, 1626, and 2930 and 2984 cm^{-1} were assigned to the -OH vibration, CH_2 bending and C=O vibrations, C=O stretching vibration of -COOH group, and CH_2 stretching vibrations, respectively.[20] The hygroscopic behavior of MSS has not been reported yet.

As shown in Fig. S2(C), during the dehydration process, a DSS droplet shrank continuously as the RH was decreased from 95% until 50.2% and effloresced at RH = 49.4%. For all particles on the image field, efflorescence took place at ERH = 44.6-50.4%, which is consistent with ERH = 46.7-47.9% observed by the EDB technique.[4] During the humidification process, the particle deliquesced at RH = 66.3%, which is consistent with DRH = 63.5-66% observed by the EDB technique,[4] higher than DRH = ~50% observed by the VSA,[19] and different from a HTDMA work showing continuous growth,[21] as summarized in Table S3. The reported discrepancy of the DRHs may be due to the different drying process employed in the VSA and HTDMA measurements from EDB and in situ RMS. The top Raman spectrum in Fig. S2(F) for the aqueous DSS droplet at RH = 90% showed peaks at 1404, 1544, and 2932 cm^{-1} for aqueous DSS and at 3450 cm^{-1} for free water, where the peaks at 1404, 1544, and 2932 cm^{-1} are for the CH_2 bending and C=O stretching bands of the $-COO^-$ group, the C=O stretching vibration, and the CH_2 stretching band, respectively.[16] The bottom Raman spectrum in Fig. S2(F) corresponds to an effloresced particle at RH = 5% and to the standard DSS powders,[22] indicating the efflorescence of DSS droplet into the DSS crystals.

D. Literature summary, including the present study, of the hygroscopic behavior of aerosols generated from NaCl and SA mixture solutions with specified molar mixing ratios

In situ Raman analysis indicated the chemical compositional evolution of the aerosols

generated from the NaCl-SA solutions during the hygroscopic measurements, forming a mixture system of NaCl, SA, and MSS due to the reaction between NaCl and SA. The DRHs and ERHs observed in this study can be regarded as those for a ternary NaCl-SA-MSS mixture system. As summarized in Table S3, three previous studies reported DRH = 71.3-72.8% for aerosols generated from a NaCl:SA = 1:1 solution;[23] DRH = 74%, 72%, and 70% for those from NaCl:SA = 6.1:1, 2:1, and 1:1.5 solutions, respectively;[24] and DRH = ~80% for those from a NaCl:SA = 2:1 solution with single-stage deliquescence,[19] which are similar to the present study. Just one ERH of aerosols generated from a NaCl:SA = 1:1 solution was previously reported to be 53.2-53.4%.[23]

E. Hygroscopic behavior and Raman spectra of glutaric acid (GA), monosodium glutarate (MSG), and disodium glutarate (DSG) aerosols

Crystalline GA can exist as two polymorphs in a thermodynamically metastable α-form and a stable β-form at room temperature.[25, 26] Fig. S3(A) presents a dehydration curve for a GA droplet and two humidification curves for α- and β-form GA particles. Among ten droplets on an image field, nine and one GA droplets crystallized as α-form and β-form particles with ERH = 13.3-40.7% and 18.8%, respectively, during the dehydration process. The top Raman spectrum in Fig. S3(D) for the aqueous GA droplet at RH = 90% shows peaks at 1300, 1417, 1442, 1710, 2932, and 2946 cm^{-1} for aqueous GA and 3460 cm^{-1} for free water, where the peaks at 1417 cm^{-1} and at 2932 and 2946 cm^{-1} were assigned to CH_2 bending and stretching vibrations, respectively, and the peak at 1710 cm^{-1} corresponds to the C=O stretching vibration of -COOH group. The second and bottom Raman spectra in Fig. S3(D) correspond to the effloresced α- and β-form particles at RH = 5%, which have different peak patterns at 1414-1464 cm^{-1} and 2914-2986 cm^{-1} and different peak positions at 1663 and 1645 cm^{-1}, where the peaks at 1663 and 1645 cm^{-1} were assigned to the C=O stretching vibrations of -COOH group.[25] During the humidification process, eight α-form and one β-form GA particles started to rearrange at RH = 77.0% and fully dissolved at DRH = 86.5(±0.5)% and 88.9%, respectively. An α-form GA particle first absorbed water at RH = 85.0-86.5%, followed by conversion to β-form and deliquescence at DRH = 88.2%. Several studies employing different hygroscopic measurement systems reported deviating DRHs of GA particles in the range of 80-93% (Table S4) except for a HTDMA report of continuous growth during the humidification process.[11, 13, 27-31] The reported deviating DRHs may be because of the formation

of different polymorphs. In contrast, an RMS study, which investigated the hygroscopic behavior of the α- and β-form GA particles, reported DRHs = 85-86% and 87-89%, respectively,[32] which is consistent with the current observations. The reported ERHs were in the range of 20-43% with one exception, which reported continuous shrinkage during the dehydration process.[13, 28-31] The current observation was ERH = 13.3-40.7% and 18.8% of the α-form and β-form, respectively, which were within the range of the ERHs reported previously. As shown in Fig. S3(A), the GA droplet showed a very small decrease in size during efflorescence, which might not be recognized in the other work.

As shown in Fig. S3(B), during the dehydration process, an MSG droplet generated from an aqueous MSG solution shrank continuously until RH = 37.9% and effloresced at ERH = 37.2%, which is also supported by the optical image and Raman spectra, even though its 2-D size increased during the phase transition. The efflorescence took place at ERH = 35.0-42.3% for all droplets on an image field. The 2-D size increase might be due to the formation of an amorphous MSG solid particle as indicated by the second Raman spectrum in Fig. S3(E). In the second Raman spectrum, the peaks at 1300 and 1710 cm^{-1} of the MSG droplet were still present, the peaks at 1417 and 1442 cm^{-1} for the droplet shifted a little bit to 1424 and 1460 cm^{-1} which are observed for MSG powders, and a small water peak at 3460 cm^{-1} can still be observed. The MSG droplet was difficult to be completely dried even when the RH was kept < 5% for a few hours; the bottom Raman spectrum in Fig. S3(E) corresponds to MSG powders obtained by the slow evaporation of an MSG solution in a desiccator for several days. During the humidification process, the MSG particle experienced a rearrangement in structure at RH = 47.6% with a decrease in size. The size increased from RH = 64.4%, where aqueous and solid phases were observed in the droplet, to DRH = 78.2%, where full deliquescence occurred as also observed in the optical images. All particles on the image field dissolved completely at DRH=78.2(±0.5)%. The Deliquescence of MSG particles occurred over a wide range of RH due to the slow mass transfer in the MSG aerosols.

As shown in Fig. S3(C), during the dehydration process, a DSG droplet generated from an aqueous DSG solution shrank continuously until effloresced at RH = 47.9%, which is supported by the change in morphology and Raman spectra, even though its 2-D size change was not distinct. The top and bottom Raman spectra in Fig. S3(F) correspond to aqueous and crystalline DSG aerosols, respectively. The efflorescence took place at ERH = 45.0-51.6% for all droplets on an image field. During the humidification process, the DSG particles dissolved completely at DRH=

65.3(±0.5)%. To the best of the authors' knowledge, this is the first study of the hygroscopic behavior of MSG and DSG particles.

F. Literature summary, including the present study, of the hygroscopic behavior of aerosols generated from NaCl and GA mixture solutions with specified molar mixing ratios

In situ Raman analysis indicated that a ternary mixture system of NaCl, GA, and MSG was investigated during the hygroscopic measurements. The DRHs of the aerosols generated from the NaCl:GA = 2:1, 1:1, and 1:2 solutions were 73.1(±0.3)%, 72.7(±0.3)%, and 71.0(±0.5)%, respectively, which are similar to each other. As summarized in Table S4, five previous studies reported DRH = ~75% for aerosols generated from NaCl:GA = 4:1, 1:1, and 1:4 solutions;[27] DRH = 57.3-70.7% for those from a NaCl:GA = 2.3:1 solution;[23] DRH = 66-75% for those from a NaCl:GA = 2.4:1 solution;[30] DRH = 72-74%, 77-81%, and 82-86% for those from NaCl:GA = 2.3:1, 1:1, and 1:2.3, respectively;[29] and DRH = 65-75%, 60-65%, and 65-70% for those from NaCl:GA = 3:1, 1:1, and 1:3, respectively, with a single deliquescence event,[28] which are comparable to the present observations. Deviating ERHs of the aerosols from NaCl-GA solutions were reported, i.e., ERH = 54.4% for NaCl:GA = 2.3:1;[23] ERH = 30-40% for NaCl:GA = 2.4:1;[30] ERH = ~45%, ~43%, and ~30-38% for those from NaCl:GA = 2.3:1, 1:1, 1:2.3, respectively;[29] and ERH = ~65%, ~60%, and continuous shrinkage for those from NaCl:GA = 3:1, 1:1, 1:3, respectively.[28] The deviating hygroscopic behavior during the dehydration process might be because the droplets generated and measured in the different systems effloresced in a kinetic and random process as the efflorescence is a rate-driven process depending on many factors.[33] Further, the various hygroscopic behavior during the dehydration process can also be attributed to the different contents of the investigated aerosols.

Table S1. Raman peaks (in cm^{-1}) for major vibration modes of DCAs and their sodium-salt aerosols.

OA			MSO		DSO		SA		MSS		DSS		GA		MSG		DSG		Vibration Mode	Ref
droplet	anhydrous	dihydrate	droplet	crystal	droplet	crystal	droplet	crystal	droplet	crystal	droplet	crystal	droplet	crystal	droplet	crystal	droplet	crystal		
1430	1306	1368	1430	1404 1445	1302 1445 1473 1580	1446 1606 1632		1277											COO	8, 17
							1243 1404	1215 1360 1407 1438	1404	1407	1404	1413	1417	1414	1417	1424	1417	1429	CH_2	16, 17, 20, 22, 25
	1472	1480																	C=O	8
		1621	1638	1634						1260	1640								O-H	1, 8, 20
1736	1702	1730	1720	1712		1740	1708	1642	1706	1626	1544	1580	1710	1663 1645	1710	1692	1560	1606	C=O	8, 6, 17, 22, 25
	2580 2910																		Combi-nations	
							2932	2920 2960	2932	2930 2984	2932	2950	2932 2946	2914 2932 2960 2986	2932 2946	2932 2870	2932 2946	2932	CH_2	16, 17, 20, 22, 25
3438		3430	3438	3424	3438		3450		3450		3450		3460		3460		3460		O-H	1

Table S2. Literature summary, including the present study, of the hygroscopic behavior of oxalic acid (OA), monosodium oxalate (MSO), disodium oxalate (DSO), and aerosols generated from NaCl and OA mixture solutions with specified molar mixing ratios. (HTDMA = Hygroscopicity tandem differential mobility analyzer; EDB = electro-dynamic balance; VSA = vapor sorption analyzer; FTIR = Fourier transform infrared spectroscopy; RMS = Raman microspectrometry; SPT = solid phase transition; CG = continuous growth; CS = continuous shrinkage; NI = not investigated)

DRH	ERH	Particle size	Particle generation	Method	Reference
Oxalic acid (OA)					
CG at RH > 45%	NI	100 nm	Dry	HTDMA	10
CG at RH > 60%	NI	50 and 100 nm	Dry	HTDMA	11
CG at RH = 10-95%	CS at RH = 40-95%	100 nm	Dry	HTDMA	2
> 90%	NI	100 nm	Dry	HTDMA	7
> 94%	51.8-56.7% (to anhydrous OA)	10-20 μm	Wet	EDB	13
> 95%; SPT at RH = ~20%	NI; SPT at RH = ~5%	Bulk	Dry	VSA	8
98%; SPT at RH =10-30%	NI	submicron	Dry/Wet	FTIR	3
> 94%; SPT at RH = 17.9-19.6%	71% (to OA dihydrate); SPT at RH = ~5%	10-20 μm	Wet	RMS	9
> 97%; SPT at RH = 20-40%	55.1-77.0% (to OA dihydrate); SPT at RH < 5%	10-15 μm	Wet	RMS	this work

Monosodium oxalate (MSO)					
> 95%;	78.1-87.1% (to MSO hydrate)	10-15 μm	Wet	RMS	this work
Disodium oxalate (DSO)					
CG at RH > 45%	NI	100 nm	Dry	HTDMA	10
> 90%	NI	100 nm	Dry	HTDMA	21
> 95%	NI	Bulk	Dry	VSA	19
> 93%	72-75.2%	~20 μm	Wet	EDB	4
> 98%	78.9-83.2%	10-15 μm	Wet	RMS	this work

NaCl:OA (mixtures)	**DRH (%)**	**ERH (%)**	**Particle size**	**Particle generation**	**Method**	**Reaction reported**	**Reference**
4.6:1.0	73%	NI	100 nm	Dry	HTDMA	NI	24
1.5:1.0	CG at RH > ~75%					Yes (Bulk ATR-FTIR)	
1.0:1.9	CG at RH > ~75%					NI	
2:1	~80%	NI	Bulk	Dry	VSA	Yes (Bulk Raman and ATR-FTIR)	19
3:1	76.0(±0.5)%	59.0-61.3%	10-15 μm	Wet	RMS	Yes	this work
2:1	76.2(±0.5)%	first ERH: 72.6-84.9% second ERH: 56.3-65.0%					
1:1	76.4(±0.3)%	first ERH: 81.7-					

		87.1% second ERH: 60.1-64.7%					
1:2	> 97%	81.7-84.4% SPT at RH = ~20%					

Table S3. Literature summary, including the present study, of the hygroscopic behavior of succinic acid (SA), monosodium succinate (MSS), disodium succinate (DSS), and aerosols generated from NaCl and SA mixture solutions with specified molar mixing ratios. (HTDMA = Hygroscopicity tandem differential mobility analyzer; EDB = electro-dynamic balance; VSA = vapor sorption analyzer; RMS = Raman microspectrometry; CG = continuous growth; CS = continuous shrinkage; NI = not investigated)

DRH	ERH	Particle size	Particle generation	Method	Reference
Succinic acid (SA)					
> 90%	NI	100 nm	Dry	HTDMA	7
> 92%	NI	100 nm	Dry	HTDMA	11
> 94%	55-59%	10-20 μm	Wet	EDB	13
> 95%	NI	Bulk	Dry	VSA	19
> 95%	84.4-90.1%	10-15 μm	Wet	RMS	this work
Monosodium succinate (MSS)					
CG at RH = 5-92%	CS at RH = 5-95%	10-15 μm	Wet	RMS	this work
Disodium succinate (DSS)					
CG	NI	100 nm	Dry	HTDMA	21
63.5-66%	46.7-47.9%	~20 μm	Wet	EDB	4
~50%	NI	Bulk	Dry	VSA	19
66.3(±0.4)%	44.6-50.4%	10-15 μm	Wet	RMS	this work

NaCl:SA (mixtures)	DRH (%)	ERH (%)	Particle size	Particle generation	Method	Reaction reported	Reference

6.1:1.0	74%	NI	100 nm	Dry	HTDMA	NI	24
2.0:1.0	72%						
1.0:1.5	70%						
1:1	71.3-72.8%	53.2-53.4%	5-10 μm	Wet	SEDB	NI	23
2:1	~80%	NI	Bulk	Dry	VSA	No (Bulk Raman)	19
2:1	74.0(±0.3)%	45.3-46.0%	10-15 μm	Wet	RMS	Yes	this work
1:1	74.2(±0.3)%	43.6-46.7%					
1:2	74.4(±0.5)%	46.0-62.8%					

Table S4. Literature summary, including the present study, of the hygroscopic properties of glutaric acid (GA), monosodium glutarate (MSG), disodium glutarate (DSG), and aerosols generated from NaCl and GA mixture solutions with specified molar mixing ratios. (HTDMA = Hygroscopicity tandem differential mobility analyzer; EDB = electro-dynamic balance; VSA = vapor sorption analyzer; FTIR = Fourier transform infrared spectroscopy; RMS = Raman microspectrometry; CG = continuous growth; CS = continuous shrinkage; NI = not investigated)

DRH	ERH	Particle size	Particle generation	Method	Reference
Glutaric acid (GA)					
CG at RH > 65%	NI	100 nm	Dry	HTDMA	11
85(±5)%	NI	100 nm	Dry	HTDMA	27
83-85%	29-33%	10-20 μm	Wet	EDB	13
~90%	~43%	5-25 μm	Wet	EDB	31
85-93%	20-30%	20-50 μm	Wet	EDB	30
~80%	CS	0.2~1.2 μm	Dry	FTIR	28
87-91%	22.5-36%	2-20 μm	Wet	Microscopy	29
85-86% (α-form)	NI	10-30 μm	Dry	RMS	32
87-89% (β-form)					
86.5(±0.5)% (α-form)	13.3-40.7% (α-form)	10-15 μm	Wet	RMS	This work
88.2-88.9% (β-form)	18.8% (β-form)				
Monosodium glutarate (MSG)					
78.2(±0.5)%	35.0-42.3%	10-15 μm	Wet	RMS	this work
Disodium glutarate (DSG)					
65.3(±0.5)%	45.0-51.6%	10-15 μm	Wet	RMS	this work

NaCl:GA (mixtures)	DRH (%)	ERH (%)	Particle size	Particle generation	Method	Reaction reported	Reference
4:1	~75%	NI	50-120 nm	Dry	TDMA	NI	27
1:1	~75%						
1:4	~75%						
2.3:1	57.3-70.7%	54.4%	5-10 µm	Wet	SEDB	NI	23
2.4:1	66-75%	30-40%	20-50 µm	Wet	EDB	NI	30
2.3:1	74(±2)%	~45%	2-20 µm	Wet	Microscopy	NI	29
1:1	79(±2)%	~43%					
1:2.3	84(±2)%	~30-38%					
3:1	65-75%	~65%	0.1~2 µm	Dry	FTIR	Yes (SEM/EDX), minor reaction	28
1:1	60-65%	~60%				minor reaction	
1:3	65-70%	CS				20-30% reaction	
2:1	73.1(±0.3)%	44.5-46.2%	10-15 µm	Wet	RMS	Yes	this work
1:1	72.7(±0.3)%	43.6-48.5%					
1:2	71.0(±0.5)%	39.9-43.9%					

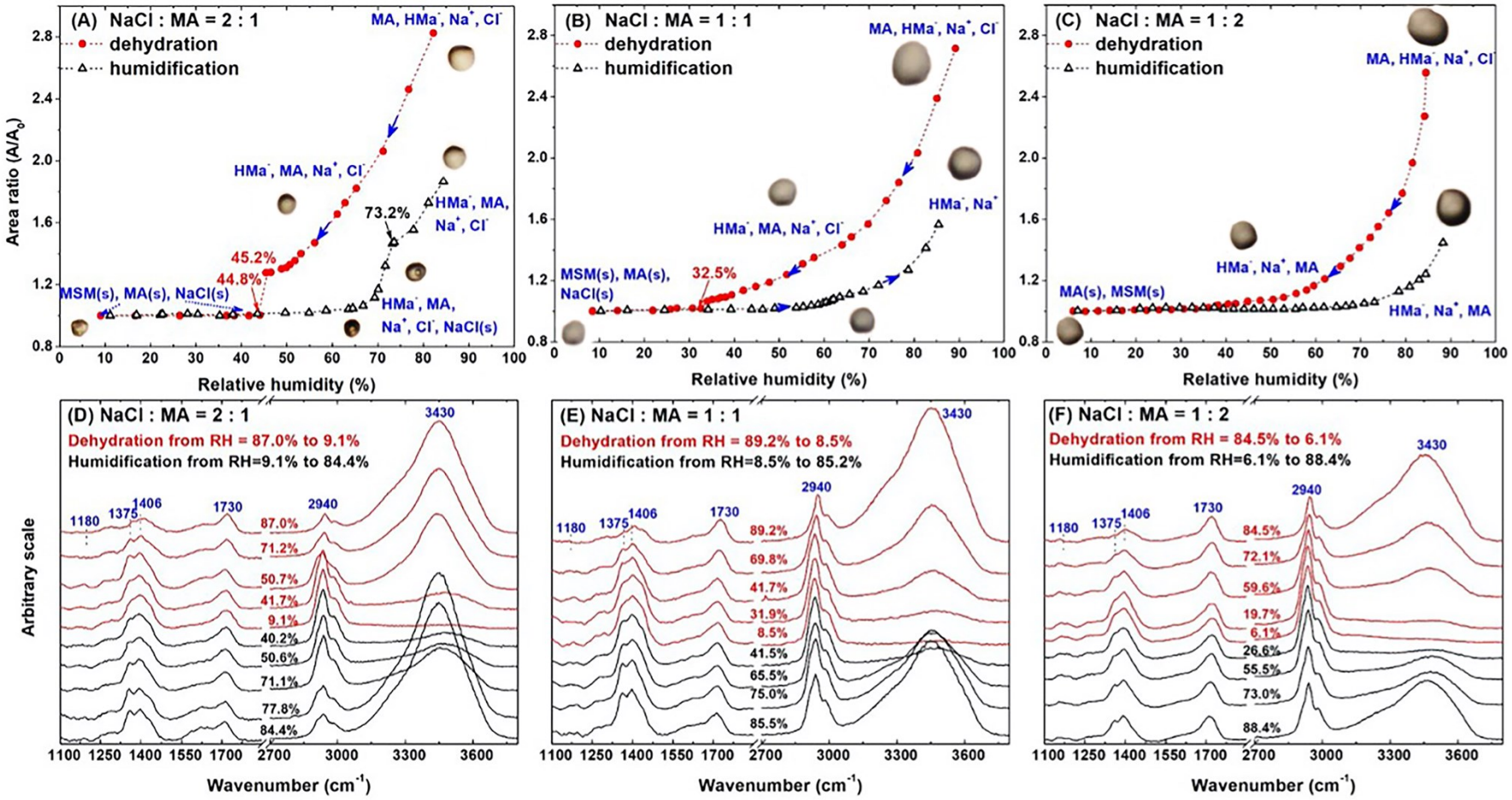

Figure S1. (A)-(C): Hygroscopic curves of NaCl:MA = 2:1, 1:1, and 1:2 aerosols, respectively. (D)-(F): Raman spectra of aerosols from NaCl-MA solutions obtained during the processes.

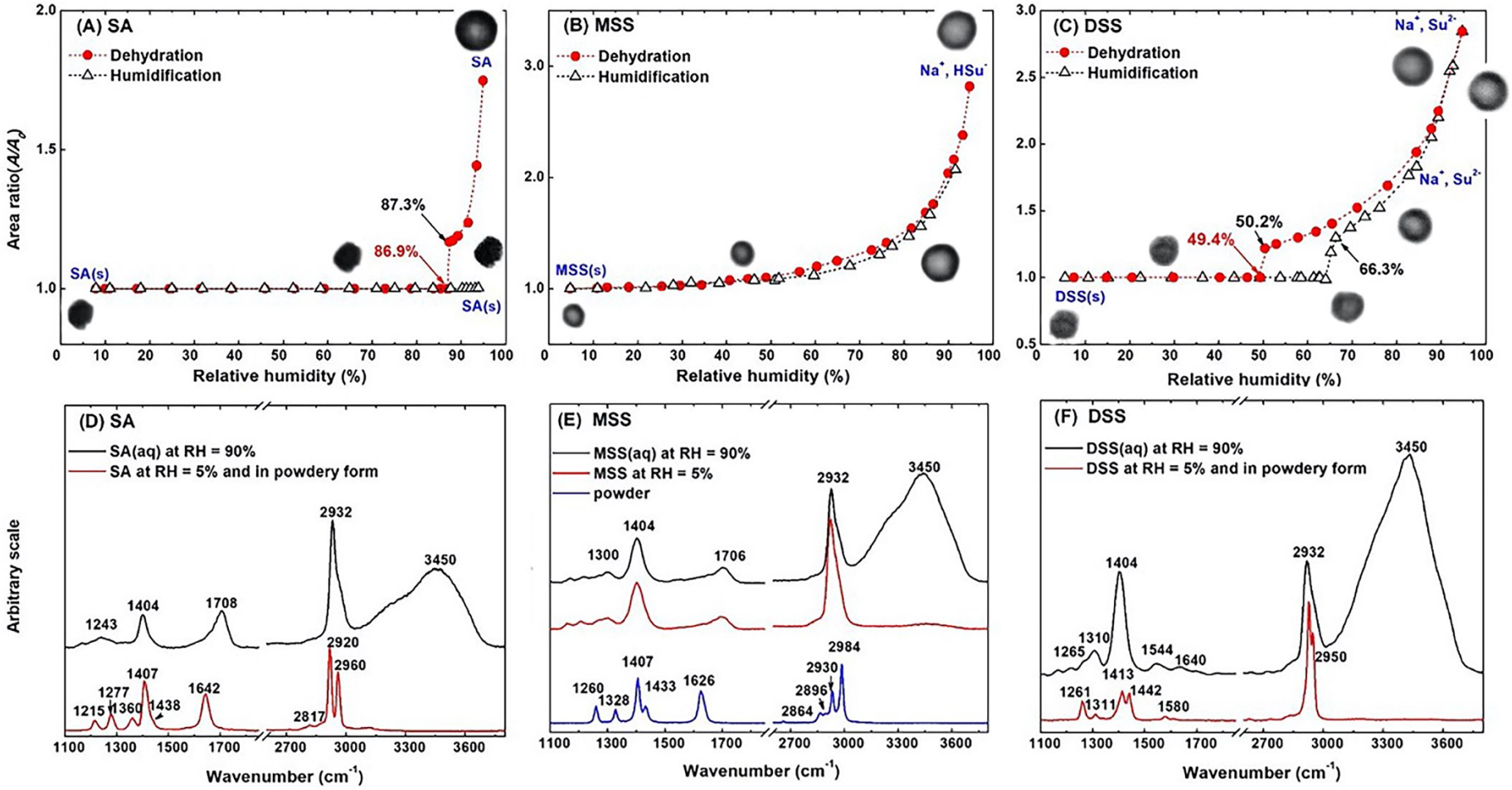

Figure S2. (A)-(C): Hygroscopic curves of pure succinic acid (SA), monosodium succinate (MSS), and disodium succinate (DSS) aerosols, respectively. (D)-(F): Raman spectra at high RH = ~90% and low RH = ~5% and for crystalline powders of SA, MSS, and DSS.

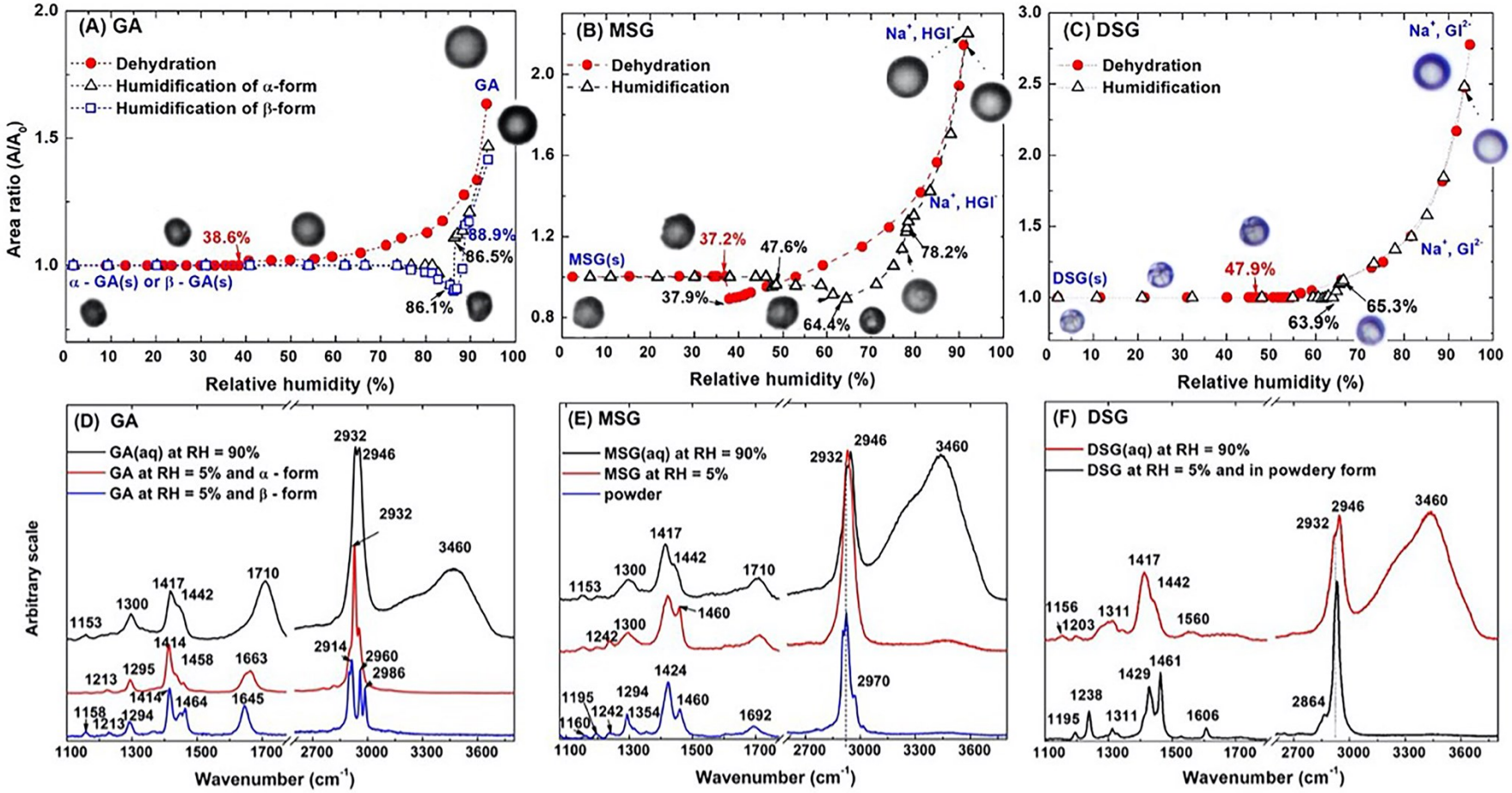

Figure S3. (A)-(C): Hygroscopic curves of pure glutaric acid (GA), monosodium glutarate (MSG), and disodium glutarate (DSG) aerosols, respectively. (D)-(F): Raman spectra at high RH = ~90% and low RH = ~5% and for crystalline powders of GA, MSG, and DSG.

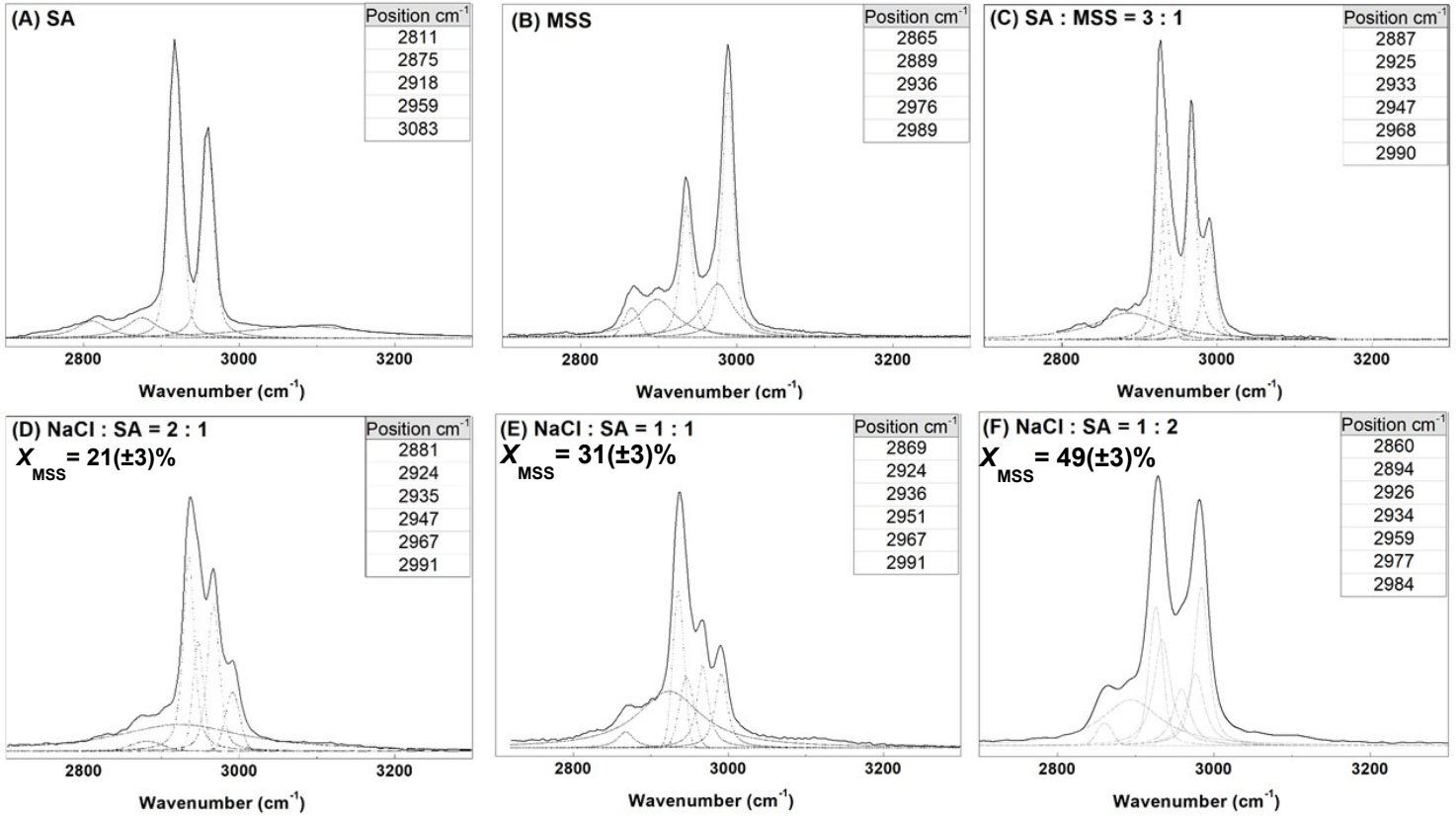

Figure S4. (A)-(F): Curve fitted Raman spectra of aerosols from SA, MSS, SA:MSS = 3:1, and NaCl:SA = 2:1, 1:1, and 1:2 solutions, respectively, at low RHs. The Raman spectra were fitted using a combined Gaussian and Lorentzian curves. Peak area ratios ($I_{2920+2960}/I_{2936+2989}$) were used to determine the contents of SA and MSS in the aerosols from NaCl:SA = 2:1, 1:1, and 1:2 solutions. (X_{MSS} = [MSS]/([MSS]+[SA]))

References

1. X. Li, D. Gupta, J. Lee, G. Park and C. U. Ro, *Environ Sci Technol*, 2017, **51**, 263-270.
2. E. Mikhailov, S. Vlasenko, S. Martin, T. Koop and U. Pöschl, *Atmospheric Chemistry and Physics*, 2009, **9**, 9491-9522.
3. C. F. Braban, M. F. Carroll, S. A. Styler and J. P. Abbatt, *The Journal of Physical Chemistry A*, 2003, **107**, 6594-6602.
4. C. Peng and C. K. Chan, *Atmospheric Environment*, 2001, **35**, 1183-1192.
5. M. E. Wise, *Journal of Geophysical Research*, 2003, **108**.
6. I. R. Zamora, A. Tabazadeh, D. M. Golden and M. Z. Jacobson, *Journal of Geophysical Research: Atmospheres*, 2011, **116**.
7. B. Jing, S. Tong, Q. Liu, K. Li, W. Wang, Y. Zhang and M. Ge, *Atmospheric Chemistry and Physics*, 2016, **16**, 4101-4118.
8. Q. Ma, H. He and C. Liu, *Atmospheric Environment*, 2013, **69**, 281-288.
9. X. Wang, B. Jing, F. Tan, J. Ma, Y. Zhang and M. Ge, *Atmospheric Chemistry and Physics*, 2017, **17**, 12797-12812.
10. S. K. R. Boreddy and K. Kawamura, *Environ Sci Process Impacts*, 2018, **20**, 1069-1080.
11. A. J. Prenni, P. J. DeMott, S. M. Kreidenweis, D. E. Sherman, L. M. Russell and Y. Ming, *The Journal of Physical Chemistry A*, 2001, **105**, 11240-11248.
12. O. Laskina, H. S. Morris, J. R. Grandquist, Z. Qin, E. A. Stone, A. V. Tivanski and V. H. Grassian, *J Phys Chem A*, 2015, **119**, 4489-4497.
13. C. Peng, M. N. Chan and C. K. Chan, *Environmental science & technology*, 2001, **35**, 4495-4501.
14. H.-J. Eom, D. Gupta, X. Li, H.-J. Jung, H. Kim and C.-U. Ro, *Analytical chemistry*, 2014, **86**, 2648-2656.
15. L. Wu, C. Becote, S. Sobanska, P.-M. Flaud, E. Perraudin, E. Villenave, Y.-C. Song and C.-U. Ro, *Atmospheric Chemistry and Physics*, 2020, **20**, 14103-14122.
16. L. Maury and L. Bardet, *Journal of Raman Spectroscopy*, 1979, **8**, 345-350.
17. M. Suzuki and T. Shimanouchi, *Journal of Molecular Spectroscopy*, 1968, **28**, 394-410.
18. S. L. Clegg and J. H. Seinfeld, *The Journal of Physical Chemistry A*, 2006, **110**, 5692-5717.
19. Q. Ma, J. Ma, C. Liu, C. Lai and H. He, *Environ Sci Technol*, 2013, **47**, 10381-10388.
20. D. Hadži, B. Orel and A. Novak, *Spectrochimica Acta Part A: Molecular Spectroscopy*, 1973, **29**, 1745-1753.
21. Z. J. Wu, A. Nowak, L. Poulain, H. Herrmann and A. Wiedensohler, *Atmospheric Chemistry and Physics*, 2011, **11**, 12617-12626.
22. R. A. Nyquist, C. L. Putzig and M. A. Leugers, *Handbook of Infrared and Raman Spectra of Inorganic Compounds and Organic Salts: Text and Explanations*, Gulf Professional Publishing, 1996.

23. M. Y. Choi and C. K. Chan, *Environmental science & technology*, 2002, **36**, 2422-2428.
24. C. Peng, B. Jing, Y. C. Guo, Y. H. Zhang and M. F. Ge, *J Phys Chem A*, 2016, **120**, 1029-1038.
25. J. Grip and E. J. Samuelsen, *Physica Scripta*, 1984, **29**, 556-560.
26. M. C. Yeung and C. K. Chan, *Aerosol Science and Technology*, 2010, **44**, 269-280.
27. C. N. Cruz and S. N. Pandis, *Environmental Science & Technology*, 2000, **34**, 4313-4319.
28. S. Ghorai, B. Wang, A. Tivanski and A. Laskin, *Environ Sci Technol*, 2014, **48**, 2234-2241.
29. A. Pant, A. Fok, M. T. Parsons, J. Mak and A. K. Bertram, *Geophysical research letters*, 2004, **31**.
30. F. D. Pope, B. J. Dennis-Smither, P. T. Griffiths, S. L. Clegg and R. A. Cox, *The Journal of Physical Chemistry A*, 2010, **114**, 5335-5341.
31. A. A. Zardini, S. Sjogren, C. Marcolli, U. Krieger, M. Gysel, E. Weingartner, U. Baltensperger and T. Peter, *Atmospheric Chemistry and Physics*, 2008, **8**, 5589-5601.
32. M. C. Yeung, T. Y. Ling and C. K. Chan, *The Journal of Physical Chemistry A*, 2010, **114**, 898-903.
33. S. T. Martin, *Chemical Reviews*, 2000, **100**, 3403-3454.